Effects of duty cycle on the characteristics of a composite surface-emitting organic distributed feedback laser

Sidney S. Yang,[1,*] Yun-Ching Chang,[1] Pei-Chun Yen,[2] and Ya-Chang Chou[2]

[1]*Institute of Photonics Technologies, National Tsing Hua University, 101, Section 2 Kuang Fu Road, Hsinchu, Taiwan 30013*
[2]*Institute of Physics, National Tsing Hua University, 101, Section 2 Kuang Fu Road, Hsinchu, Taiwan 30013*
**Corresponding author: ssyang@ee.nthu.edu.tw*

Received January 19, 2007; revised April 26, 2007; accepted April 29, 2007;
posted May 15, 2007 (Doc. ID 79074); published July 19, 2007

Based on the coupled-wave theory, we model the periodic structure and analyze the influence on composite surface-emitting organic distributed feedback (DFB) lasers. Second-order DFB gratings with duty cycles of 0.3, 0.5, and 0.7 patterned by electron-beam lithography were fabricated. The composite active layer consisted of 4-(dicyanomethylene)-2-tert-butyl-6-(1,1,7,7-tetramethyljulolidin-4-yl-vinyl)-4H-pyran (DCJTB) and poly(N-vinylcarbazole) (PVK) spin-cast on a textured surface. Excited with 532 nm laser pulses, different lasing characteristics and threshold pumping fluences are exhibited. These are explained by the discrepancy in the coupling coefficients and the threshold gains calculated from the proposed model. © 2007 Optical Society of America

OCIS codes: 140.2050, 140.3490, 160.4890.

1. INTRODUCTION

Over the past few years a considerable number of studies have been concentrated on organic thin-film lasers [1,2]. It has been shown that organic molecules and conjugated polymers possess potential as emitting gain material. By means of well-designed laser cavities, especially with periodic structures such as distributed feedback (DFB) resonators [3], distributed Bragg reflectors (DBR) [4], and two-dimensional photonics crystals (PhCs) [5], a few research groups have introduced various types of optical pumped organic thin-film lasers of high efficiency. Such devices also show promising results due to the fact that the periodic structure provides narrow linewidth, frequency stability, high slope efficiency and low lasing threshold.

However, for DFB based organic thin-film lasers, only a few attempts [6]—to the best of our knowledge—have been made at investigating the effect on the emission characteristics of the cavity structure. In this paper, we focus on the performance with respect to duty cycle of second-order organic DFB lasers in a composite system. Via the coupled-wave theory [7,8], simulated data are also presented to analyze the emission characteristics of our devices.

2. THEORETICAL MODEL

The Bragg equation is commonly applied to estimate the emission wavelength λ_B of a typical one-dimensional DFB laser with certain period Λ and effective refractive index n_{eff}. However, the emission characteristics can be analyzed in detail via the coupled-wave theory developed by Kogelnik and Shank [7,9]. Here, we adopt the theory assuming low edge reflection.

The contradirectional traveling waves ($\vec{E}_R$ and $\vec{E}_L$) of a specific wavelength λ are coupled and oscillate inside the cavity. The behavior of the coupled fields can be modeled as

$$-\frac{d\vec{E}_R}{dz} + (g - j\delta)\vec{E}_R = j\kappa\vec{E}_L,$$

$$\frac{d\vec{E}_L}{dz} + (g - j\delta)\vec{E}_L = j\kappa\vec{E}_R, \tag{1}$$

where $\delta(=2n_{eff}\pi/\lambda - 2n_{eff}\pi/\lambda_B)$ and g are, respectively, known as the detuning and gain coefficient. κ, the coupling coefficient, is a real number in a purely index-coupled device fabricated by spin-casting [8–10]. A DFB laser with higher coupling coefficient possesses stronger optical feedback. For a periodic structure with rectangular teeth, an approach introduced by Streifer *et al.* in calculating the coupling coefficient was adopted, as shown in Fig. 1 [11,12]. We simplified the corrugated structure of refractive index n_i (here $i=1$, air; $i=2$, active layer, and $i=3$, substrate), period Λ, duty cycle $D=w/\Lambda$, depth d, and thickness t, to a three-layer planar waveguide that consisted of air, equivalent active layer with effective refractive index n_{eff} and effective thickness $t'=t+(1-D)d$, and the substrate [8,11,12]. Because the weakly confined TM wave (lower effective refractive index in the active area) builds up slower in the gain medium and therefore has higher threshold pumping fluence, we consider only the TE wave. The coupling coefficient of an mth order DFB cavity can be described as [11]

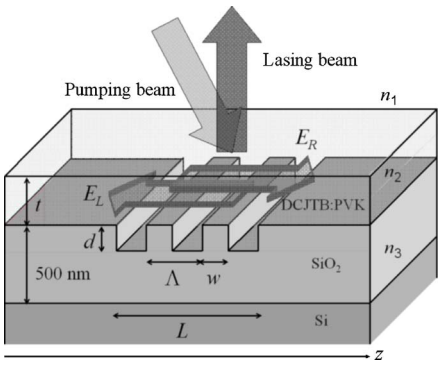

Fig. 1. Structure of 1-D organic DFB laser.

$$\kappa = \frac{k_0^2(n_1^2 - n_2^2)}{4\pi\beta m N^2}\sin(m\pi D)\left\{g_2 + \frac{\sin(2g_2h)}{2h}[1-\cos(2g_2h)] + \frac{q^2}{h^2}\left[g_2 - \frac{\sin(2g_2h)}{2h}\right] + \frac{1}{q}[1-\exp(-2g_1q)]\right\}, \quad (2)$$

where $q=\sqrt{\beta^2-n_1^2k_0^2}$, $h=\sqrt{n_2^2k_0^2-\beta^2}$, $p=\sqrt{\beta^2-n_3^2k_0^2}$, $g_1=Dd$, and $g_2=(1-D)d$. β is the propagation constant of the traveling wave that propagates in the equivalent active layer. The threshold gain g_{th} of each TE longitudinal mode of a DFB laser with grating length L and coupling coefficient κ can also be obtained by solving the eigenequation

$$\kappa\sinh(\gamma L) = \pm j\gamma, \quad (3)$$

where γ is the complex propagation constant obtained by $\gamma^2=\kappa^2+(g_{th}-j\delta)^2$ [7]. Considering a relatively flat emission spectrum around Bragg wavelength, the longitudinal mode with the lowest threshold gain g_{th} will reach the lasing condition first as the pumping fluence increases. Other modes that fail to reach the threshold condition will be suppressed and provide only background spontaneous emission.

3. FABRICATION AND SIMULATION

Three pieces of 500 nm thick thermally grown silicon dioxide wafers with a 200 μm $\times$ 400 μm corrugation area of the same period (Λ=400 nm) and the same etched depth (d=100 nm) were structured by electron-beam lithography and the dry etching process (Fig. 2). Duty cycles of corrugation areas were 0.3, 0.5, and 0.7. We adopted a composite active layer consisting of 4-(dicyanomethylene)-2-tertbutyl -6-(1,1,7,7-tetramethyljulolidin-4-yl-vinyl)-4H-pyran (DCJTB) and poly(N-vinylcarbazole) (PVK).

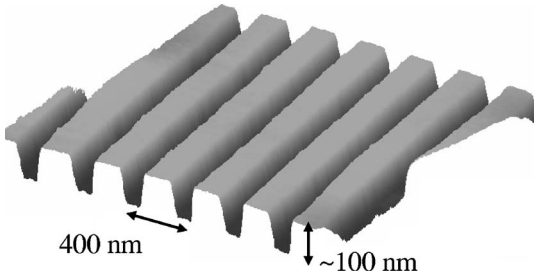

Fig. 2. Periodic corrugation measured by atomic force microscopy.

The chemical structures are shown in Fig. 3. DCJTB has shown superior amplified sponteneous emission characteristics to those of the commonly used dye DCM (more than three times the gain, less than a third of the loss, and lower than 25 times the threshold in the host of polystyrene) [13,14]. For the device with period Λ of 400 nm, effective refractive index (n_{eff}) $\approx$1.53 (n_{SiO_2}=1.457 and $n_{DCJTB:PVK}$=1.637), and the Bragg order m=2, we estimated the Bragg wavelength λ_B to be 612 nm—near the emission peak of DCJTB (Fig. 3)—by means of the Bragg condition ($2n_{eff}\Lambda=m\lambda_B$). PVK and DCJTB (97:3) were dissolved in chloroform with concentration 2% by weight. We spin-cast the solution on a textured substrate with speed 2500 rpm for 20 s. The thickness of the coated active layers t was measured to be 250 nm by the surface profiler.

The photoluminescent spectrum of DCJTB-doped PVK (3% wt) planar thin-film in the visible region ranges from wavelengths of 550 nm to 700 nm and has a maximum at 600 nm (Fig. 3). Since PVK shows no emission or absorption in the visible range, the output emission can be attributed mainly to DCJTB. With the DFB structure, the lasing spectrum is confined to a comparably narrow band around 620 nm.

In our study, we focused on second-order (m=2) DFB lasers whose propagation direction of the emitting laser beam is perpendicular to the surface of the DFB structure. By means of Eq. (2), we plotted the coupling coefficients as a function of duty cycle with various tooth heights [Fig. 4(a)]. The simulated data show that κ becomes larger as the corrugated depth increases up to 200 nm. Coupling coefficients are also strongly dependent on duty cycle. For a second-order DFB structure with various depths d, the coupling coefficient κ has a local maximum when the duty cycle $\approx$0.77 or 0.28. The coupling efficiency is highest when the duty cycle is 0.77, but zero when the duty cycle is 0.5. As is indicated in the figure, the coupling coefficients of the real devices we made are 449.7 cm^{-1} for D=0.3 and 610.3^{-1} for D=0.7.

Figure 4(b) shows the relationship between the threshold gain and the detuning coefficient of the devices with grating length L of 200 μm. For fixed L, the higher the coupling coefficient (the stronger the optical feedback), the lower the threshold gain. For the devices with D=0.3 and 0.7, the calculated threshold gains g_{th} are 18.4 cm^{-1} and 11.2 cm^{-1}, respectively, corresponding to coupling coefficients of 449.7 cm^{-1} and 610.3 cm^{-1}.

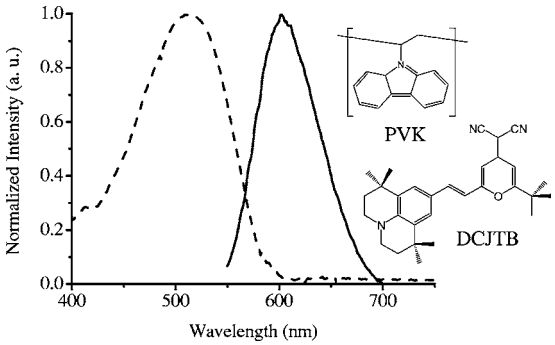

Fig. 3. Absorption (dashed curve) and emission spectra (solid curve) of DCJTB and molecular structures of DCJTB and PVK.

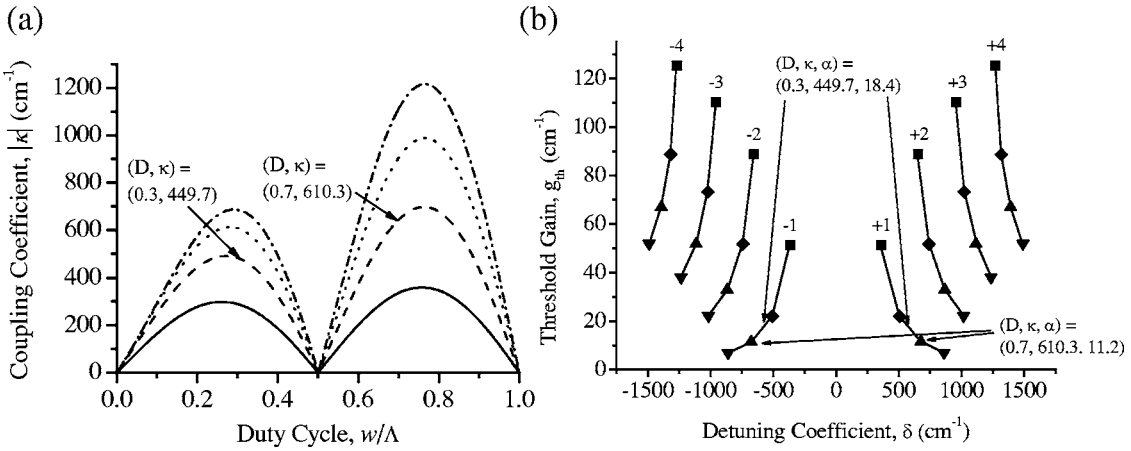

Fig. 4. (a) Simulation result of coupling coefficient κ versus duty cycle D with different etched depth d: $d=50$ nm (solid curve), $d=100$ nm (dashed curve), $d=150$ nm (dotted curve), $d=200$ nm (dotted-dashed curve). (b) Simulation result of threshold gain g_{th} versus detuning factor δ with different coupling coefficient κ: $\kappa=200\ \mathrm{cm}^{-1}$ (filled squares), $\kappa=400\ \mathrm{cm}^{-1}$ (filled diamonds), $\kappa=600\ \mathrm{cm}^{-1}$ (filled upright triangles), and $\kappa=800\ \mathrm{cm}^{-1}$ (filled inverted triangles) (here $m=2$, $n_{SiO_2}=1.457$, $n_{DCJTB:PVK}=1.637$, $\Lambda=400$ nm, and $t=250$ nm).

4. MEASUREMENT RESULTS AND DISCUSSION

Since the maximum absorption of DCJTB occurs at the wavelength of 530 nm (Fig. 3), a Q-switched second-harmonic generation (SHG) Nd:YAG laser delivering 7 ns pulses at 50 Hz was chosen to be the pumping source ($\lambda=532$ nm). We focused the pumping beam on the active layer. The diameter of the spot size was approximately 200 μm. The incident angle of the pumping beam was set to 45°. We used a pair of polarizers to control the energy of the pump pulse. The output characteristics were recorded via a fiber-coupled CCD spectrometer.

Emission spectra of devices with different duty cycles under various pumping fluences are shown in Fig. 5. The device with $D=0.3$ shows spontaneous emission under low pumping fluence $\epsilon=143\ \mu\mathrm{J/cm}^2$ [Fig. 5(a)]. As we increase the pumping fluence, the output energy slowly increases. Until reaching the threshold pumping fluence, 220 $\mu\mathrm{J/cm}^2$ as indicated in Fig. 6, the emission shows a rapidly rising peak at 620.6 nm. Another longitudinal mode is observed at 630 nm when the pumping fluence is continuously increased to 390 $\mu\mathrm{J/cm}^2$. Those two modes define the stop band width as 9.2 nm. Compared with the previous case, the device with $D=0.5$ shows difficulty in lasing. The emission spectrum remains similar at low pumping levels. The stimulated emission peak can be observed only at the highest pumping fluence [Fig. 5(b)].

The device with $D=0.7$ shows the best lasing capability at a wavelength of 624.8 nm [Fig. 5(c)]. However, longitudinal modes on the long wavelength side cannot be observed even under the highest pumping fluence in our experiments. This can be explained as follows. For a given mode, δ increases as κ gets larger as indicated in 4(b). Since the device with $D=0.7$ has the highest κ, the cavity allows longitudinal modes on the long wavelength side to detune further from the wavelength, with the highest spontaneous emission cross section shown in Fig. 3. Therefore, the material's gain is not high enough to reach the threshold gain to achieve the lasing condition.

Figure 6 presents the laser output characteristics for

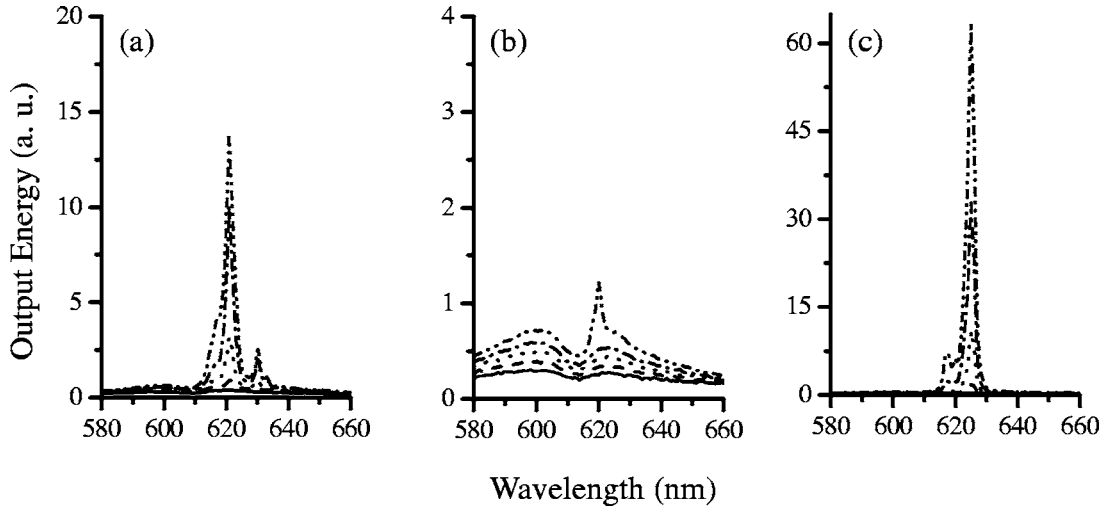

Fig. 5. Emission spectra of devices with different duty cycles (D) under various pumping fluences ϵ[=143 $\mu\mathrm{J/cm}^2$ (solid curves), 203 $\mu\mathrm{J/cm}^2$ (dashed curves), 264 $\mu\mathrm{J/cm}^2$ (dotted curves), 324 $\mu\mathrm{J/cm}^2$ (dashed–dotted curves), and 391 $\mu\mathrm{J/cm}^2$ (dashed–double dotted curves)]: (a) $D=0.3$, (b) $D=0.5$, and (c) $D=0.7$.

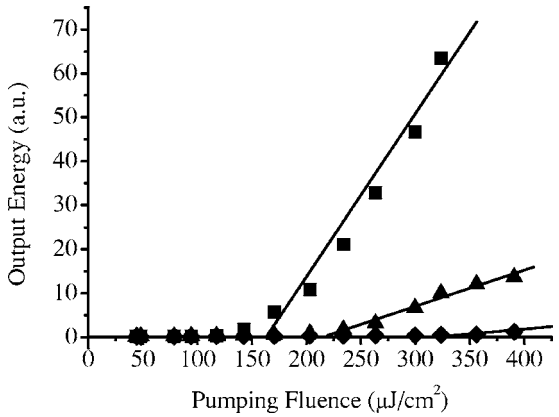

Fig. 6. Emission characteristics and fitted lines with different duty cycles: $D=0.3$ (filled triangles), $D=0.5$ (filled diamonds), and $D=0.7$ (filled squares).

different duty cycles. Possessing lowest threshold gain g_{th}, the device with $D=0.7$ has not only the lowest threshold pumping fluence but also the best slope efficiency. The threshold pumping fluences of devices with $D=0.3$, 0.5, and 0.7 are, respectively, 220, 320, and 170 μJ/cm^2, corresponding to the material's estimated gain of 22.4 cm^{-1}, 31.1 cm^{-1}, and 17.9 cm^{-1}, respectively. The values of the material's gain are measured by the method of amplified spontaneous emission [15,16].

Although the duty cycle of the device cannot be fabricated to be exactly at 50%, high threshold pumping fluence and threshold gain associated with low coupling coefficient are observed. For devices with $D=0.3$ and 0.7, the calculated threshold gains are, respectively, 18.4 cm^{-1} and 11.2 cm^{-1}, which are different from the experimental material's gain under the respective pumping energy of 220 and 170 μJ/cm^2. The differences between the experimental and calculated values are mainly due to the absorption loss from the Si layer beneath the SiO_2 substrate. By replacing with transparent materials, such as glass, the extra loss could be prevented. The threshold pumping fluence is not as low as previously reported [17], since the concentration of the molecules contributing to emission (DCJTB) is only 3 wt.% in the whole active layer. Increasing the concentration of DCJTB or mixing in energy transfer agents, the threshold pumping fluence could be further reduced.

Figure 7 shows the emitting laser beam shape projected on the screen when we pumped a device with $D=0.7$. The sample surface was placed on the yz plane. The pumping beam was incident at 45° to the x axis on the xy plane. The emitting laser beam propagated along the $-x$ direction, and its angular divergence was measured as 9 mrad. The polarization of the pumping beam had little effect on either the energy or the polarization of the emitting laser beam, since the orientation of the organic molecules was randomly distributed via the spin-casting process.

5. CONCLUSION

A composite system consisting of DCJTB/PVK is first introduced as the active medium of a surface emitting organic DFB laser. A model based on the coupled-wave theory is proposed. We solve the effective propagation constants β in the equivalent active layers of second-order DFB lasers with different duty cycles. Via Eq. (2) the coupling coefficients κ of each device are calculated ($\kappa=449.7$ cm^{-1} for $D=0.3$ and $\kappa=610.3$ cm^{-1} for $D=0.7$). Considering a nonreflecting grating edge, we take κ and the grating length L into Eq. (3) and finally obtain the threshold gains g_{th} of 18.4 cm^{-1} and 11.2 cm^{-1} for the device $D=0.3$ and $D=0.7$, respectively. We also observe the significant variation in threshold pumping fluences ϵ_{th} between two devices from the experimental data ($\epsilon_{th}=170$ μJ/cm^2 and 220 μJ/cm^2 for $D=0.3$ and 0.7, respectively). Although the exact value of κ (~ 0) is not calculated for our device with $D=0.5$, the highest threshold pumping fluence, 320 μJ/cm^2, is expected and observed. It is evident that the higher coupling coefficient indeed contributes to the lower threshold gain and the correspondingly lower threshold pumping fluence.

The model based on the coupled-wave theory is validated and provides an optimum duty cycle of 0.77 while the coated thickness is $\approx$50 to 250 nm for typical spin-cast second-order DFB organic lasers. Our finding indicates that the coupled-wave theory might be generally applicable in optimizing coating thickness, etched depth, grating length, and other specifications in organic DFB lasers.

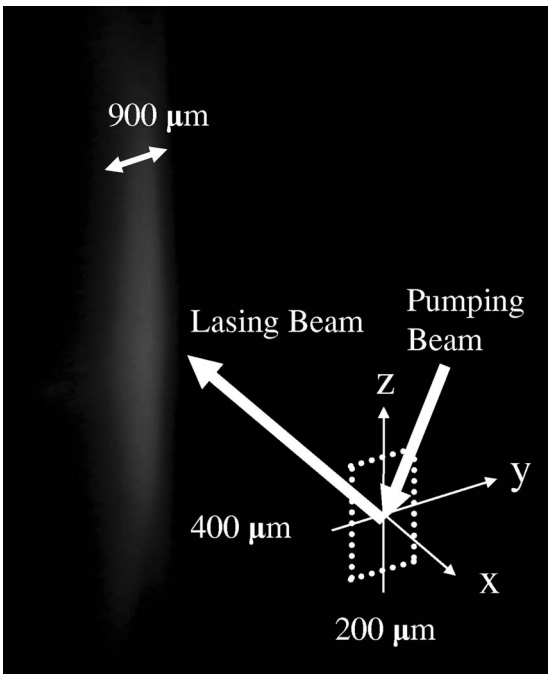

Fig. 7. Schematic drawing of the device setup and image of output beam shape.

ACKNOWLEDGMENTS

The authors are grateful to National Science Council of Taiwan (NSC 95-2221-E-007-199) and Ministry of Economic Affairs, Taiwan (95-EC-12-A-08S1-042) for financial support.

REFERENCES

1. N. Tessler, G. J. Denton, and R. H. Friend, "Lasing from conjugated-polymer microcavities," Nature (London) **382**, 695–697 (1996).
2. V. G. Kozolov, V. Bulovic, P. E. Burrows, and S. R. Forrest, "Laser action in organic semiconductor waveguide and double-heterostructure devices," Nature (London) **389**, 362–364 (1997).
3. C. Kallinger, M. Hilmer, A. Haugeneder, M. Perner, W. Spirkl, U. Lemmer, J. Feldmann, U. Scherf, K. Müllen, A. Gombert, and V. Wittwer, "A flexible conjugated polymer laser," Adv. Mater. (Weinheim, Ger.) **10**, 920–923 (1998).
4. A. Dodabalapur, M. Berggren, R. E. Slusher, Z. Bao, A. Timko, P. Schiortino, E. Laskowski, H. E. Katz, and O. Nalamasu, "Resonators and materialsfor organic lasers based on energy transfer," IEEE J. Sel. Top. Quantum Electron. **4**, 67–74 (1998).
5. G. A. Turnbull, P. Andrew, W. L. Barnes, and I. D. W. Samuel, "Operating characteristics of a semiconducting polymer laser pumped by a microchip laser," Appl. Phys. Lett. **82**, 313–315 (2003).
6. G. A. Turnbull, A. Carleton, G. F. Barlow, A. Tahraouhi, T. F. Krauss, K. A. Shore, and I. D. W. Samuel, "Influence of grating characteristics on the operation of circlar-grating distributed-feedback polymer lasers," J. Appl. Phys. **98**, 0231051–7 (2005).
7. H. Kogelnik and C. V. Shank, "Coupled-wave theory of distributed feedback lasers," J. Appl. Phys. **43**, 2327–2335 (1972).
8. A. Yariv, "Coupled-mode theory for guided-wave optics," IEEE J. Quantum Electron. **QE-9**, 919–933 (1973).
9. H. Kogelnik and C. V. Shank, "Stimulated emission in a periodic structure," J. Appl. Phys. **18**, 152–154 (1971).
10. S. Riechel, U. Lemmer, J. Feldmann, T. Benstem, W. Kowalsky, U. Scherf, A. Gombert, and V. Wittwer, "Laser modes in organic solid-state distributed feedback lasers," Appl. Phys. B B **71**, 897–900 (2000).
11. W. Streifer, D. R. Scifres, and R. D. Burnham, "Coupling coefficients for distributed feedback single- and double-hetrostructure diode lasers," IEEE J. Quantum Electron. **QE-11**, 867–873 (1975).
12. R. D. Burnham, D. R. Scifres, and W. Streifer, "Single-heterostrucutre distributed-feedback GaAs-diode lasers," IEEE J. Quantum Electron. **QE-11**, 439–449 (1975).
13. C. H. Chen, J. Shi, and K. P. Klubek, "Red organic electroluminescent materials," US patent 5908521 (1999).
14. W. Lu, B. Zhong, and D. Ma, "Amplified spontaneous emission and gain from optically pumped films of dye-doped polymers," Opt. Lett. **26**, 5074–5078 (2004).
15. K. L. Shaklee and R. F. Leheny, "Direct determination of optical gain in semiconductor crystal," Appl. Phys. Lett. **18**, 475–477 (1971).
16. M. D. McGehee, R. Gupta, S. Veenstra, E. K. Miller, M. A. Díaz-García, and A. J. Heeger, "Amplified spontaneous emission from photopumped films of a conjugated polymer," Phys. Rev. B **58**, 7035–7039 (1998).
17. T. Riedl, T. Rabe, H.-H. Johannes, W. Kowalsky, J. Wang, T. Weimann, P. Hinze, B. Nehls, T. Farrell, and U. Scherf, "Tunable organic thin-film laser pumped by an inorganic violet diode laser," Appl. Phys. Lett. **88**, 241161-3 (2006).